

pubs.acs.org/ac Letter

Nanobody-Based Microfluidic Immunosensor Chip Using Tetraphenylethylene-Derived Covalent Organic Frameworks as Aggregation-Induced Electrochemiluminescence Emitters for the Detection of Thymic Stromal Lymphopoietin

Yue Jia, Min Zhu, Xiaoyue Zhang, Dehao Jia, Tian Tian, Binnan Shi, Zhuangzhuang Ru, Hongmin Ma,* Yakun Wan,* and Qin Wei*



Cite This: Anal. Chem. 2024, 96, 10116-10120



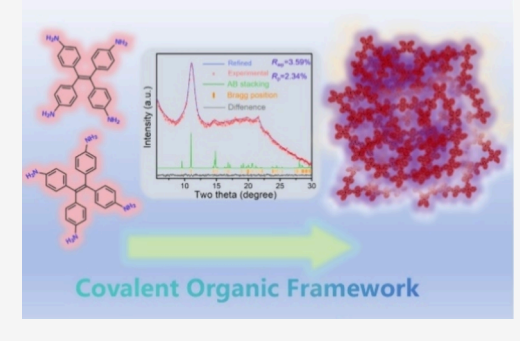
ACCESS I

III Metrics & More

Article Recommendations

Supporting Information

ABSTRACT: In this letter, a sensitive microfluidic immunosensor chip was developed using tetrakis(4-aminophenyl)ethene (TPE)-derived covalent organic frameworks (T-COF) as aggregation-induced electrochemiluminescence (AIECL) emitters and nanobodies as efficient immune recognition units for the detection of thymic stromal lymphopoietin (TSLP), a novel target of asthma. The internal rotation and vibration of TPE molecules were constrained within the framework structure, forcing nonradiative relaxation to convert into pronounced radiative transitions. A camel-derived nanobody exhibited superior specificity, higher residual activity and epitope recognition postcuring compared to monoclonal antibodies. Benefiting from the affinity between silver ions (Ag⁺) and cytosine (C), a double-stranded DNA (dsDNA) embedded with Ag⁺ was modified onto the surface of TSLP. A positive correlation was obtained between



the TSLP concentration (1.00 pg/mL to 4.00 ng/mL) and ECL intensity, as Ag^+ was confirmed to be an excellent accelerator of the generation of free radical species. We propose that utilizing COF to constrain luminescent molecules and trigger the AIECL phenomenon is another promising method for preparing signal tags to detect low-abundance disease-related markers.

he sensitivity, reproducibility, and stability of electrochemiluminescence (ECL) immunosensors directly depend on the type of emitters, antibodies, and carriers used in the sensor design. 1 Although ECL-based immunosensors have yielded satisfactory results in the detection of various biomarkers, the extensive limitations faced during the selection of luminophores, sensing substrates, immune molecules, and other sensing units are unacceptable. Along with high ECL efficiency, traditional luminophores such as ruthenium complexes, luminol and its derivatives, quantum dots, carbon nitride nanosheets, etc., when encapsulated or adsorbed on electrode surfaces, can lead to unpredictable molecular leakage issues.2 More importantly, the irreversible aggregation-caused quenching (ACQ) effect arising from $\pi - \pi$ stacking among the mentioned planar molecules should be emphasized, causing signal reduction or even disappearance.³ Electrode chemical modification technology relies on the electronic diffusion between solid-state electrochemically active materials and liquid electrolytes at the solid-liquid interface rather than on a simple homogeneous system.⁴ De Cola et al. discovered aggregation-induced ECL (AIECL) in 2017, attracting attention to the development of novel ECL luminophores. Unlike the ACQ effect, the AIECL phenomenon exhibits enhanced ECL efficiency in the aggregated or solid state

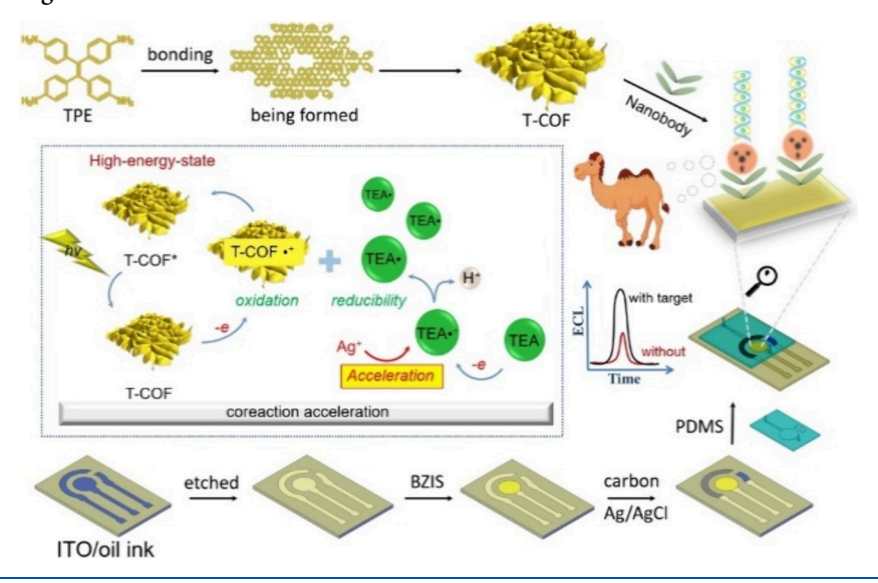
compared to the dispersed state, which is precisely what ECLbased biosensors require. It is easy to imagine that many luminophores, such as poorly hydrophilic complexes and organic compounds, now possess greater potential applications. Among them, tetraphenylethylene and its derivatives with size-tunable luminescence have emerged as the most promising AIECL emitters owing to their unique phenylethylene structure and π -electron conjugated system.⁶ Currently, considerable efforts have been made to modify tetraphenylethylene molecules to trigger the AIECL effect, for example, nanomaterial and biomimetic encapsulation with spatial confinement effects, coordination-induced formation of crystalline framework materials, and self-assembly of metalorganic gels.⁷⁻⁹ It is hypothesized that covalent organic frameworks (COFs) offer a unique platform for researchers to study the AIECL phenomenon of tetraphenylethylene and its derivatives; particularly, two-dimensional (2D) COFs

Received: May 5, 2024 Revised: June 7, 2024 Accepted: June 9, 2024 Published: June 10, 2024





Scheme 1. Schematic Diagram of Fabrication of TSLP Microfluidic Immunosensor



provide an ideal path for molecular recognition using continuous nanometer-scale channels and aligned active binding sites. ^{10,11} Only a few reports have documented the fluorescence behavior of tetraphenylethylene-based COFs to date, with no one delving into exploration of their ECL performance.

The selection and use of biorecognition elements also directly impact the sensitivity and accuracy of immunosensors. 12,13 Monoclonal antibodies are susceptible to external stimuli and may undergo irreversible structural damage when used in sensor construction. Researchers discovered a nanobody in the camel serum that lacks the light chain and CH1 regions in the heavy chain, serving as a minimal fragment naturally present in the binding of the antigen. 14 It possesses unique stability, specificity, and simplicity in humanization and a robust ability for epitope recognition and binding, almost perfectly overcoming the limitations of traditional antibodies. It can also firmly bind to solid-phase carriers at high densities, avoiding interference from complex samples, and is suitable for capturing trace target molecules. 15 To commercialize portable immunosensors, their miniaturization and real-time on-site analysis are crucial steps that cannot be overlooked. Traditional sensor construction relies on the manual layer-by-layer modification of signal targets and sensing units on conductive materials such as glassy carbon electrodes (GCEs). The variability between sensor batches resulting from this operation is unacceptable for the precise detection of targets. However, microfluidic immunosensor chips fabricated via screen printing processes and microfluidic technology offer the advantages of miniaturization and automation, integrating fluid control technology and sensing elements. These chips can address these issues and improve sensor performance.¹⁰

Herein (Scheme 1), thymic stromal lymphopoietin (TSLP)-specific nanobodies with high affinity were successfully separated from an immune phage—display nanobody library via camel immunization, lymphocyte isolation, RNA extraction, and library construction. tetrakis(4-aminophenyl)ethene (TPE) was utilized as the main molecule to prepare T-COF under mild conditions, which exhibited strong ECL emission in the presence of triethylamine (TEA) coreactant. All detection processes are integrated into a microfluidic sensor chip, and with the coreaction accelerator silver ion (Ag^+) , a

feasible TSLP detection method has been established by comparing with enzyme-linked immunosorbent assay (ELISA) method.

X-ray diffraction (XRD) analysis and theoretical structural simulations on Materials Studio were performed to define the crystalline structure of T-COF. According to theoretical structural simulations and Pawley refinements, T-COF can be fitted into the AB stacking model with corresponding unit cell parameters of a=6.3436 Å, b=9.8125 Å, c=16.6144 Å, $\alpha=85.63^{\circ}$, $\beta=77.75^{\circ}$, and $\gamma=68.98^{\circ}$ in the P1 space group. The residual factors, $R_p=2.34\%$ and $R_{wp}=3.59\%$, demonstrate the reliability of the computational model (Figures 1a and 1b). The XRD pattern of T-COF shows peaks at 11.06° , 14.87° , and 17.9° , which are assigned to the (011), (1 1 0), and (1 0–1) planes, respectively. 17,18

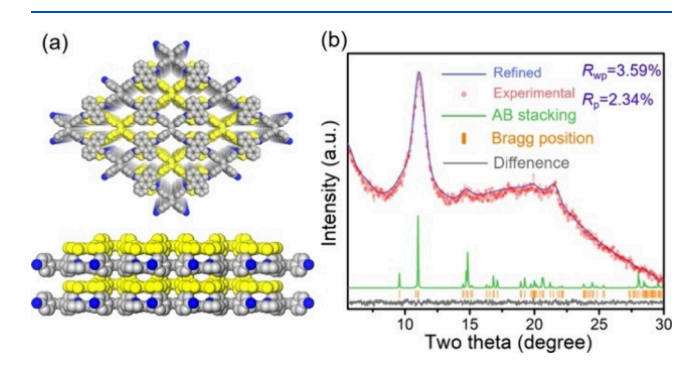


Figure 1. (a) Structures of T-COF. (b) Experimental (red dot) and simulated (blue line) XRD patterns of T-COF.

As a novel AIECL emitter, the emission mechanism of T-COF should be first explored. As shown in eqs S1 and S2, the TEA coreactant and T-COF emitter lose electrons to generate TEA• and T-COF• radical cations, respectively, as confirmed by the cyclic voltammetry (CV) scans shown in Figure 2a. The initial potential of 0.44 V corresponds to the preliminary oxidation of TEA, while the peak at 0.84 V corresponds to the electron loss oxidation of T-COF. To further validate this value, density functional theory (DFT) was used to simulate the highest occupied molecular orbital (HOMO) of T-COF, and the calculation results shown in

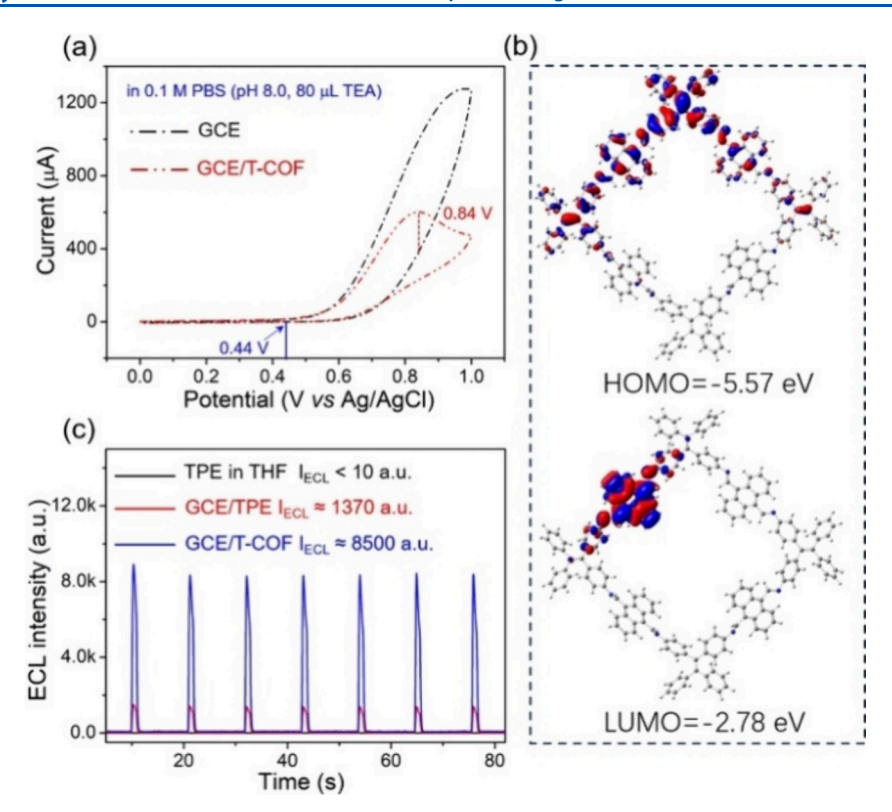


Figure 2. (a) CV curves of the bare GCE and GCE/T-COF. (b) Frontier molecular orbitals with the corresponding HOMO and lowest unoccupied molecular orbital energy levels of T-COF. (c) AIECL effect verified via ECL-time curves.

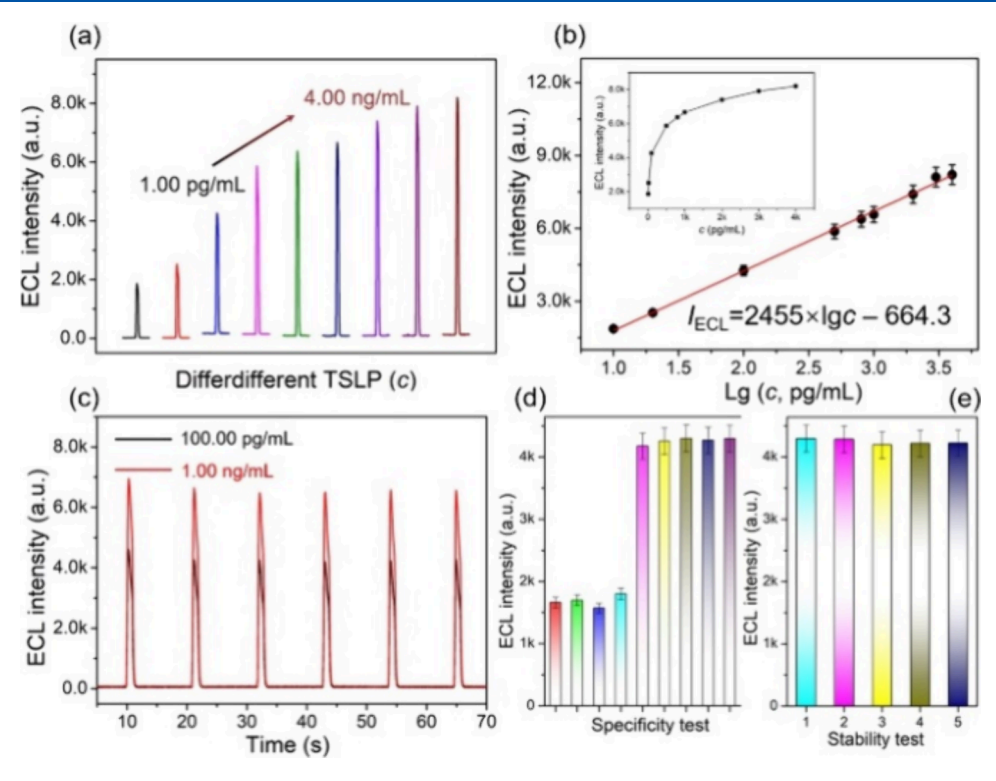


Figure 3. (a) Positive correlation between the ECL intensity and TSLP concentration in the range from 1.00 pg/mL to 4.00 ng/mL and (b) corresponding point plot and linear fitting curve of the ECL intensity and target concentration. (c) Signal output stability tests using 100.00 pg/mL and 1.00 ng/mL TSLP as targets, respectively. (d) Specificity tests using 100.00 ng/mL TSLP as the target and 500.00 ng/mL of the interferent containing CRP, SP, Ig E, and LTS. (e) Reproducibility tests using 100.00 ng/mL TSLP as the target. Error bars: \pm standard deviation (SD), n = 5.

Figure 2b revealed it to be 5.57 eV below the vacuum level, resulting in the theoretical oxidation potential of T-COF

calculated as 0.82 V (eq S6), which closely aligns with 0.84 V.¹⁹ Additionally, the generation of TEA•+ can be effectively

accelerated in the presence of Ag⁺ in the system, as confirmed by the electron paramagnetic resonance (EPR) results in Figure S1. Subsequently, TEA•⁺ can deprotonate to generate an ion radical with strong reducibility in an alkaline environment (eq S3), which can undergo redox reactions with T-COF•⁺ to afford the high-energy state of T-COF* (eq S4). Accompanied by the release of photons, a strong ECL signal can be obtained (eq S5). It is important to emphasize that in the aforementioned process, the release of ECL benefits from the rigid structure of COF, restricting the free rotation triggered AIECL effect of the tetraphenylethylene group. Homogeneous ECL emission of monomeric liquid TPE, and pure solid-state TPE cannot exhibit such a strong signal as shown in Figure 2c.

After verifying the successful construction of the immunosensor via electrochemical impedance spectroscopy (for more details, see Supporting Information (SI)), the proposed sensing strategy was tested to recognize TSLP under optimal conditions. Figure 3a demonstrates the clear signal response of the sensor to TSLP in the concentration range from 1.00 pg/ mL to 4.00 ng/mL. A line graph similar to a logarithmic function curve is plotted in the inset of Figure 3b, in which the ECL intensity as vertical axis and TSLP concentration as horizontal axis. To further investigate the relation between the ECL intensity and target concentration, we logarithmically transformed the TSLP concentrations using a base value of 10. Then, the obtained values were plotted on the horizontal axis and the ECL intensity was plotted on the vertical axis, resulting in the linear curve shown in Figure 3b. The equation of this curve is $I_{ECL} = 2455 \times \lg c - 664.3$ (R² = 0.998), and a low limit of detection (LOD) of 2.72 pg/mL was calculated.

The stability of immunosensor relates to data retrieval, which is an important indicator for the newly established sensing method. To assess the stability of the signal output, 100.00 pg/mL and 1.00 ng/mL TSLP were selected as targets in the low- and high-concentration regions, respectively, and consecutive ECL excitations and emissions were performed (Figure 3c). The ECL signals were collected, and their relative standard deviations were calculated (RSD), which are 3.3% and 2.1%, respectively. These values are considered "satisfactory" in analytical chemistry, demonstrating the good signal output stability of our biosensors. Importantly, the sensing specificity determines whether accurate detection of target samples can be achieved to avoid false positives caused by other interfering substances in the sample. In specificity testing, 500.00 ng/mL C-reactive protein (CRP), serum perforin (SP), immunoglobulin E (Ig E), and leukotriene (LTS) were selected as four interfering substances, which were tested alone or mixed with 100.00 ng/mL TSLP. As shown in Figure 3d, the sensor shows no response to the target in the absence of TSLP, but the signal intensity is comparable to the ECL intensity (indicated by 100.00 ng/mL TSLP in Figure 3b) in the presence of TSLP, with an RSD of 1.1%, confirming that these sensors show good specificity. Finally, five sensors from the same and different batches of many products were used to detect 100.00 ng/mL TSLP. Figure 3e shows that the signal difference in these five sensors is minimal (RSD = 0.9%), which is important evidence for the good reproducibility of the as-proposed analytical method.

Unlike standard antigens, the compositions of body fluids (e.g., serum, cerebrospinal fluid, and urine) are complex including various proteins, fats, sugars, inorganic salts, vitamins, etc., and their concentrations are much higher

compared to many trace targets.²⁰ These factors affect the sensitivity and accuracy of a new method for detecting lowabundance disease-related targets. To dispel this doubt and evaluate the clinical application value of the new method, we compared it with the standard method of enzyme linked immunosorbent assay (ELISA) and conducted spiked recovery experiments in the serum of healthy adults and asthma patients. As shown in Table S4, the concentrations of TSLP in the serum of healthy and asthma individuals are 87.20 pg/mL and 372.00 pg/mL, respectively, based on authoritative reports provided by the hospital. Subsequently, standard TSLP concentrations of 30.00 pg/mL, 90.00 pg/mL, and 200.00 pg/mL were spiked into samples from healthy samples. The results show that the spiked recovery rates are between 96.6% and 99.3%. Additionally, the precision of this method is not significantly different from the ELISA method (confidence level = 95%), as the values obtained from the *F*-test are <6.39. Furthermore, the values from the t-test are <2.31 with a total degree of freedom of 8, indicating that there is no significant systematic error between the proposed method and ELISA method. Focusing on the analysis data in serum samples from asthma patients, standard TSLP concentrations of 130.00 ng/ mL, 400.00 ng/mL, and 850.00 ng/mL were added. The recovery rate of this method ranges from 98.8% to 99.8%. For the three samples at a 95% confidence level, the F-test values are <6.39. Additionally, the maximum value is 2.21 in the *t*-test with a total degree of freedom of 8. These results collectively demonstrate the high precision and accuracy of the proposed method, confirming its feasibility in detecting trace amounts of TSLP in different types of serum samples.

In summary, it is a feasible method for inducing AIECL behavior by preparing COF between emitter and organic guest. The development of advanced sensor devices such as microfluidic chips carriers, and nanobody units has become an important step in the process of independent research and development of disease marker diagnostic products. This study provides a feasible strategy for detecting low-abundance disease-related biomarkers.

ASSOCIATED CONTENT

Supporting Information

The Supporting Information is available free of charge at https://pubs.acs.org/doi/10.1021/acs.analchem.4c02347.

Chemicals, apparatus, and experimental details, Figures S1–S6 and Table S1–S4, characterization of TSLP-specific nanobody, calculation of ECL efficiency, and characterization of biosensor construction (PDF)

AUTHOR INFORMATION

Corresponding Authors

Qin Wei — Key Laboratory of Interfacial Reaction & Sensing Analysis in Universities of Shandong, School of Chemistry and Chemical Engineering, Collaborative Innovation Center for Green Chemical Manufacturing and Accurate Detection, University of Jinan, Jinan 250022, P. R. China; Department of Chemistry, Sungkyunkwan University, Suwon 16419, Republic of Korea; orcid.org/0000-0002-3034-8046; Email: sdjndxwq@163.com

Yakun Wan — Shanghai Novamab Biopharmaceuticals Co., Ltd., Shanghai 201318, China; Email: ykwan@ novamab.com

Hongmin Ma — Key Laboratory of Interfacial Reaction & Sensing Analysis in Universities of Shandong, School of Chemistry and Chemical Engineering, Collaborative Innovation Center for Green Chemical Manufacturing and Accurate Detection, University of Jinan, Jinan 250022, P. R. China; ◎ orcid.org/0000-0002-7061-8944; Email: mahongmin2002@126.com

Authors

- Yue Jia Key Laboratory of Interfacial Reaction & Sensing Analysis in Universities of Shandong, School of Chemistry and Chemical Engineering, Collaborative Innovation Center for Green Chemical Manufacturing and Accurate Detection, University of Jinan, Jinan 250022, P. R. China; ⊚ orcid.org/0000-0002-2336-4486
- Min Zhu Shanghai Novamab Biopharmaceuticals Co., Ltd., Shanghai 201318, China
- Xiaoyue Zhang Key Laboratory of Interfacial Reaction & Sensing Analysis in Universities of Shandong, School of Chemistry and Chemical Engineering, Collaborative Innovation Center for Green Chemical Manufacturing and Accurate Detection, University of Jinan, Jinan 250022, P. R. China
- Dehao Jia Key Laboratory of Interfacial Reaction & Sensing Analysis in Universities of Shandong, School of Chemistry and Chemical Engineering, Collaborative Innovation Center for Green Chemical Manufacturing and Accurate Detection, University of Jinan, Jinan 250022, P. R. China
- Tian Tian Key Laboratory of Interfacial Reaction & Sensing Analysis in Universities of Shandong, School of Chemistry and Chemical Engineering, Collaborative Innovation Center for Green Chemical Manufacturing and Accurate Detection, University of Jinan, Jinan 250022, P. R. China
- Binnan Shi Key Laboratory of Interfacial Reaction & Sensing Analysis in Universities of Shandong, School of Chemistry and Chemical Engineering, Collaborative Innovation Center for Green Chemical Manufacturing and Accurate Detection, University of Jinan, Jinan 250022, P. R. China
- Zhuangzhuang Ru Key Laboratory of Interfacial Reaction & Sensing Analysis in Universities of Shandong, School of Chemistry and Chemical Engineering, Collaborative Innovation Center for Green Chemical Manufacturing and Accurate Detection, University of Jinan, Jinan 250022, P. R. China

Complete contact information is available at: https://pubs.acs.org/10.1021/acs.analchem.4c02347

Author Contributions

"Yue Jia and Min Zhu contributed equally to this work.

Notes

The authors declare no competing financial interest.

ACKNOWLEDGMENTS

This study was supported by the National Natural Science Foundation of China (22274062, 22206056), the Natural Science Foundation of Shandong Province (ZR2022QB117), the Shanghai Pudong New Area Science and Technology Development Fund Industry-University-Research Special Project (PKX2022-S04), and Shanghai Science and Technology Innovation Action Plan - cell and gene therapy special project (23J21901800). The authors thank Fan Li from Shiyanjia Lab

(www.shiyanjia.com) for the DFT analysis. Thanks to eceshi (www.eceshi.com) for the EPR test.

REFERENCES

- (1) Makaraviciute, A.; Ramanaviciene, A. *Biosens. Bioelectron.* **2013**, 50, 460-471.
- (2) Carrara, S.; Arcudi, F.; Prato, M.; De Cola, L. Angew. Chem., Int. Ed. 2017, 56 (17), 4891–4891.
- (3) Zhang, Y.; Zhao, Y.; Han, Z.; Zhang, R.; Du, P.; Wu, Y.; Lu, X. Angew. Chem., Int. Ed. 2020, 59 (51), 23261–23267.
- (4) Jia, Y.; Zhang, N.; Du, Y.; Ren, X.; Ma, H.; Wu, D.; Fan, D.; Wei, Q.; Ju, H. Biosens. Bioelectron. 2022, 210, No. 114291.
- (5) Carrara, S.; Aliprandi, A.; Hogan, C. F.; De Cola, L. *J. Am. Chem. Soc.* **2017**, 139 (41), 14605–14610.
- (6) Liu, J.; Zhang, H.; Hu, L.; Wang, J.; Lam, J. W. Y.; Blancafort, L.; Tang, B. Z. J. Am. Chem. Soc. **2022**, 144 (17), 7901-7910.
- (7) Jia, Y.; Ren, X.; Zhang, X.; Wu, D.; Ma, H.; Li, Y.; Wei, Q. Anal. Chem. 2023, 95 (24), 9139–9144.
- (8) Li, H.; Zhu, Y.; Zhang, J.; Chi, Z.; Chen, L.; Su, C.-Y. RSC Adv. **2013**, 3 (37), 16340–16344.
- (9) Shi, Y.; Wang, S.; Tao, W.; Guo, J.; Xie, S.; Ding, Y.; Xu, G.; Chen, C.; Sun, X.; Zhang, Z.; He, Z.; Wei, P.; Tang, B. Z. Nat. Commun. 2022, 13 (1), 1882.
- (10) Dey, A.; Rahimi, F. A.; Barman, S.; Hazra, A.; Maji, T. K. J. Mater. Chem. **2023**, 11 (25), 13615–13622.
- (11) Dong, J.; Pan, Y.; Yang, K.; Yuan, Y. D.; Wee, V.; Xu, S.; Wang, Y.; Jiang, J.; Liu, B.; Zhao, D. ACS Nano **2022**, 16 (2), 2355–2368. (12) Gao, Y.; Zeng, Y.; Liu, X.; Tang, D. Anal. Chem. **2022**, 94 (11),
- (12) Gao, Y.; Zeng, Y.; Liu, X.; Tang, D. Anal. Chem. **2022**, 94 (11), 4859–4865.
- (13) Yu, Z.; Gong, H.; Xu, J.; Li, Y.; Zeng, Y.; Liu, X.; Tang, D. Anal. Chem. **2022**, 94 (7), 3418–3426.
- (14) Barakat, S.; Berksöz, M.; Zahedimaram, P.; Piepoli, S.; Erman, B. Free Radical Bio. Med. 2022, 182, 260-275.
- (15) Muyldermans, S. Applications of Nanobodies. 2021, 9, 401-421.
- (16) Krone, K. M.; Warias, R.; Ritter, C.; Li, A.; Acevedo-Rocha, C. G.; Reetz, M. T.; Belder, D. J. Am. Chem. Soc. **2016**, 138 (7), 2102–2105
- (17) Faheem, M.; Aziz, S.; Jing, X.; Ma, T.; Du, J.; Sun, F.; Tian, Y.; Zhu, G. J. Mater. Chem. A 2019, 7 (47), 27148–27155.
- (18) She, P.; Qin, Y.; Wang, X.; Zhang, Q. Adv. Mater. 2022, 34 (22), 2101175.
- (19) Cardona, C. M.; Li, W.; Kaifer, A. E.; Stockdale, D.; Bazan, G. C. Adv. Mater. **2011**, 23 (20), 2367–2371.
- (20) Wu, D.; Tang, J.; Yu, Z.; Gao, Y.; Zeng, Y.; Tang, D.; Liu, X. Anal. Chem. **2024**, 96 (21), 8740–8746.